RNA profiles in different cell lineages from the CNS for more precise interpretation of selective neuronal death in FUS-associated ALS/FTLD.

We reported recently that FUS regulates a subset of exon splicing events and gene expression in mouse primary cortical neurons in a position-dependent manner[20]. We also showed scattered binding of FUS to and around alternatively spliced exons, including those associated with neurodegeneration, such as *Mapt*, *Camk2a*, and *Fmr1*[20]. In the present study, we extend our research to the global roles of FUS on RNA metabolism in different cell lineages from the different CNS regions, including primary motor neurons, cortical neurons, glial cells, and cerebellar neurons, and describe a new pathomechanism of FUS-related ALS/FTLD.

Results

Lentivirus-mediated silencing of *FUS* in different cell lineages from the CNS. We have described recently the establishment of Fus-silenced primary cortical neurons[20]. In order to compare RNA profiles of FUS in different cell types of the CNS, we prepared Fus-silenced primary motor neurons, primary cerebellar neurons, and primary glial cells by introducing lentivirus-expressing shRNA against Fus (shFUS) or scrambled control (Fig. 1A). The purity of each primary cell culture was confirmed by immunostaining for cell specific markers. We successfully established primary cultures of motor and cortical neurons with more than 95% purity. For primary glial cell cultures, we obtained astroctyes with purity of more than 95%, as confirmed by staining for GFAP. Both Purkinje cells and granule cells were the main cell populations among primary cerebellar neurons (Fig. 1B).

To exclude possible off-targeting effects, we used two different shRNAs, shFUS1 and shFUS2 in experiments performed in triplicate, as described in our recent study[20]. Correlation analysis between shFUS1 and shFUS2 showed a coefficient of determination (R^2) of 0.93 in primary cortical neurons, indicating that these two shRNA have minimal off-targeting effects[20]. The expression levels of *Fus* mRNA were efficiently suppressed in all four types of cells by both shFUS1 and shFUS2 by real-time quantitative PCR (Supplementary Fig. S1A). The FUS protein levels were decreased in all four types of cells by both shFUS1 and shFUS2 by immunoblot (Supplementary Fig. S1B). Immunohistochemistry also showed markedly decreased FUS protein levels in all four primary cells infected with shFUS1 and shFUS2 compared to shRNA against control scrambled oligonucleotides (shCont) (Supplementary Fig. S1C).

Innate gene expression profiles in neurons and glial cells. The innate gene expression profiles of each cell-type infected with shCont were analyzed using the Affymetrix Mouse Exon 1.0 ST Array and compared by principal component analysis. The correlation coefficients were calculated (Supplementary Table S1) and summarized in the correlation plot and 2D-PCA scores (Fig. 1C). We found that the expression profiles of cerebellar neurons are very close to those of cortical neurons. The expression profiles of motor neurons are also similar to those of cortical neurons but with a lesser extent. On the other hand, the expression profiles of glial cells were divergent from those of the other three neuronal cells.

FUS regulates gene expressions in motor neurons, cortical neurons, and glial cells, but to a lesser extent in cerebellar cells. In the next step, we analyzed the gene expression and alternative splicing events in Fus-silenced and control primary cells using the Affymetrix Mouse Exon 1.0 ST Array. To identify the common effects of Fus-silencing in different cell lineages from the CNS, we compiled a list of differentially expressed genes and differentially spliced exons in primary motor neurons, cortical neurons, glial cells, and cerebellar neurons, in which shFUS was introduced (GEO accession numbers: GSE36153 for cortical neurons, GSE42421 for motor neurons, glial cells, and cerebellar neurons). We first prepared a list of FUS-regulated genes which were differentially expressed by shFUS for each cell lineage by filtering the gene-level signal intensities with t-test p values of ≤ 0.1. Then, we identified differentially expressed genes shared among the four primary types of cells.

The results of plot analysis of gene expression in primary cells of the CNS after Fus-depletion are shown in Fig. 2A. The numbers of differentially expressed genes with more than 1.3-fold change were higher in primary cortical neurons, motor neuron, and glial cells than in cerebellar neurons. Indeed, there were more than 2000 differentially expressed genes in these three cell types but only 494 genes in primary cerebellar neurons (Supplementary Table S2).

FUS-mediated gene expression profiles are similar between cortical and motor neurons and are less similar when these neuronal cells are compared to cerebellar neurons. We investigated the similarity in differential gene expression profiles regulated by FUS among primary motor, cortical, and cerebellar neurons. Venn diagrams indicated overlap in genes or exons whose expression was regulated in the same direction by FUS (t-test, $p < 0.1$). Both motor and cortical neurons which are destined to die in ALS/FTLD, shared appreciable proportions of gene expression profiles (775/2321, 33.4% of genes in motor neurons; 775/2470, 31.4% of genes in cortical neurons). Cerebellar neurons, which are considered to be spared in ALS/FTLD, contained fewer numbers of FUS-regulated genes (t-test, $p < 0.1$) than motor and cortical neurons, and showed small overlapping rate with other neurons (58/494, 11.7% of genes with motor neurons; and 50/494, 10.1% of genes with cortical neurons) (Fig. 2B). The fold-changes in overlapped genes filtered by the t-test ($p < 0.1$) were plotted for primary motor, cortical, and cerebellar neurons. Comparison of gene expression profiles showed significantly high correlations between motor and cortical neurons ($R^2 > 0.80$, Fig. 2C: $p \leq 0.1$, by t-test, Supplementary Fig. S2A: $p \leq 0.075$ and 0.05, by t-test).

FUS-mediated alternative splicing profiles are similar in cortical and motor neurons but largely divergent compared with cerebellar neurons. We next investigated the similarity in differential alternative splicing profiles regulated by FUS among primary motor, cortical, and cerebellar neurons. We filtered the exon-level signal intensities with t-test p values ≤ 0.1, and prepared a list of FUS-regulated exons for each cell lineage and identified shared FUS-regulated exons. In alternative splicing profiles, about 10% (965/10727, 9.0% of genes in motor neurons; and 965/8183, 11.8% of genes in cortical neurons) of genes showed overlap between motor and cortical neurons at the exon levels, whereas cerebellar neurons showed only overlap in about 4% (434/9907, 4.4% of genes with motor neurons; and 325/9907, 3.3% of genes with cortical neurons) of genes at the exon levels compared with the other two neurons (Fig. 2B). The overlapped exons filtered by the t-test were also plotted for primary motor, cortical, and cerebellar neurons. Comparisons of exon splicing profiles showed a significant correlation only between motor and cortical neurons ($R^2 > 0.7$), but not between motor and cerebellar neurons, or cortical and cerebellar neurons ($R^2 < 0.1$, each) (Fig. 2C: $p \leq 0.1$, by t-test, Supplementary Fig. S2B: $p \leq 0.075$ and 0.05, by t-test).

Glial cells are similar to motor and cortical neurons in FUS-regulated gene expression profiles but not in alternative exon profiles. Glial cells, which are thought to be the modifier in ALS/FTLD, were also investigated with regard to similarity to motor and cortical neurons in differential gene expression and alternative splicing profiles regulated by FUS. Venn diagrams showed that the gene expression profiles of glial cells shared certain similarities with motor and cortical neurons (422/2074, 20.3% of genes with motor neurons; 453/2074, 21.8% of genes with cortical neurons, Fig. 2D). Comparison of gene expression profiles in the plot analysis showed positive correlations between glial cells and both motor and cortical

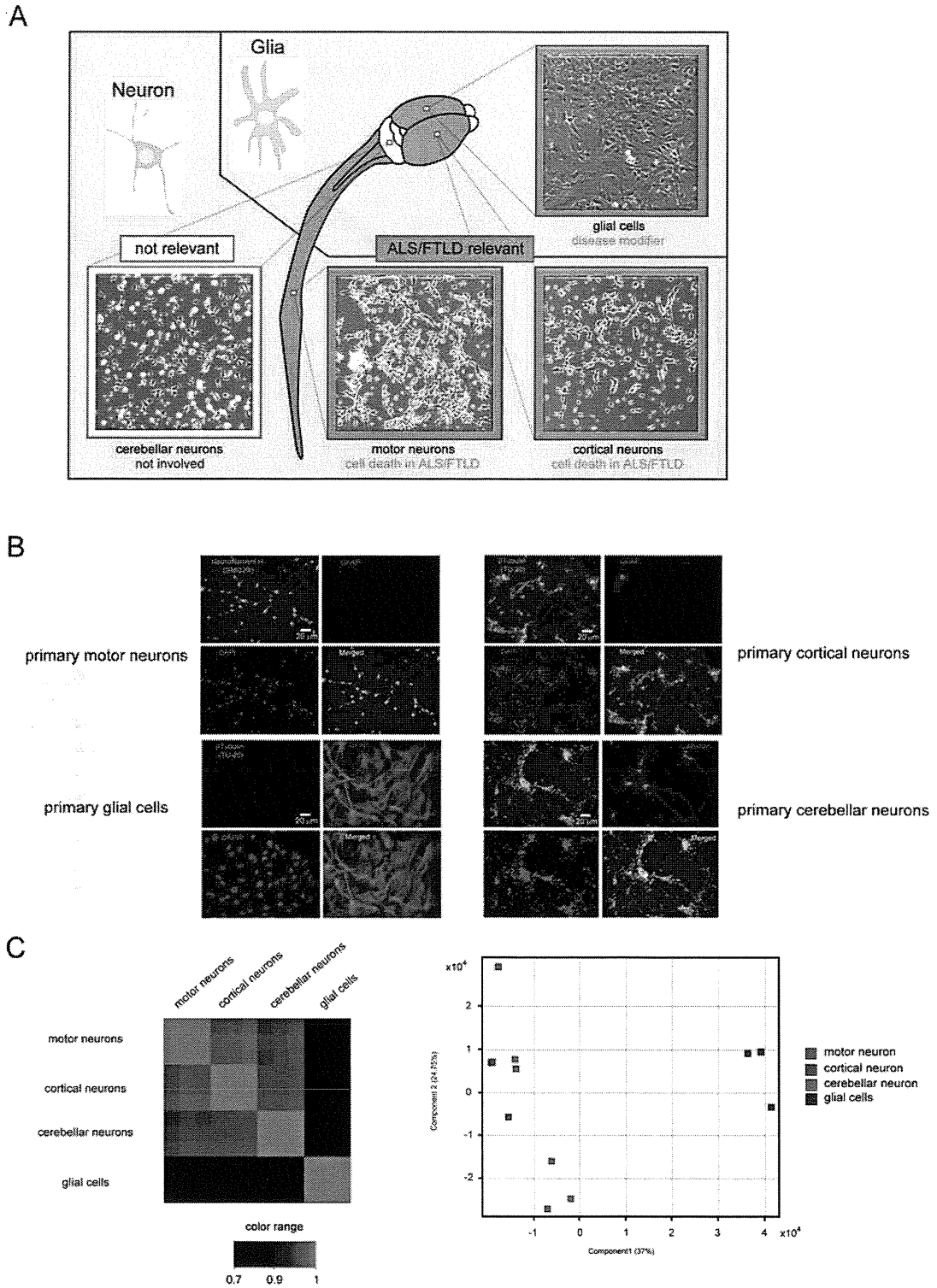

Figure 1 | Experimental schema and characterization of four primary cells from the central nervous system. (A) Primary motor neurons were harvested from the spinal cords of C57BL/6 mouse embryos at embryonic E13. Primary cortical neurons and primary glial cells were obtained from the cerebrum of C57BL/6 mouse at E15. Primary cerebellar neurons were obtained from the cerebellum of C57BL/6 mouse at E15. Motor and cortical neurons, but not cerebellar neurons, are affected in ALS/FTLD. Glial cells are disease-modifiers in ALS/FTLD. Primary cells were infected with lentivirus expressing two different shRNAs against FUS (shFUS1 and shFUS2) and control shRNA (shCont). Total RNA was isolated and analyzed by the Affymetrix Mouse Exon Array. Each experiment was performed in triplicate. (B) The purity of primary motor neurons, primary cortical neurons, primary glial cells, and primary cerebellar neurons was confirmed by immunostaining using specific antibodies: anti-neurofilament-H antibody (SMI32R) for primary motor neurons; anti-β tubulin antibody (TU20) for primary cortical neurons; anti-GFAP antibody for glial cells; anti-Zic1 antibody for granule cells in primary cerebellar neurons; and anti-calbindin antibody for Purkinje cells in primary cerebellar neurons. (C) The innate gene expression profiles of each cell type introduced with shCont were compared by principal component analysis (n = 3 for each cell-type). The correlation coefficients were calculated (Supplementary Material, Table S1) and summarized in the correlation plot (left). The 2D PCA scores and the loadings plots of the innate gene expression profiles of each cell-type introduced with shCont indicated that significant separation between the profiles of the three primary neurons and that of glial cells (right).

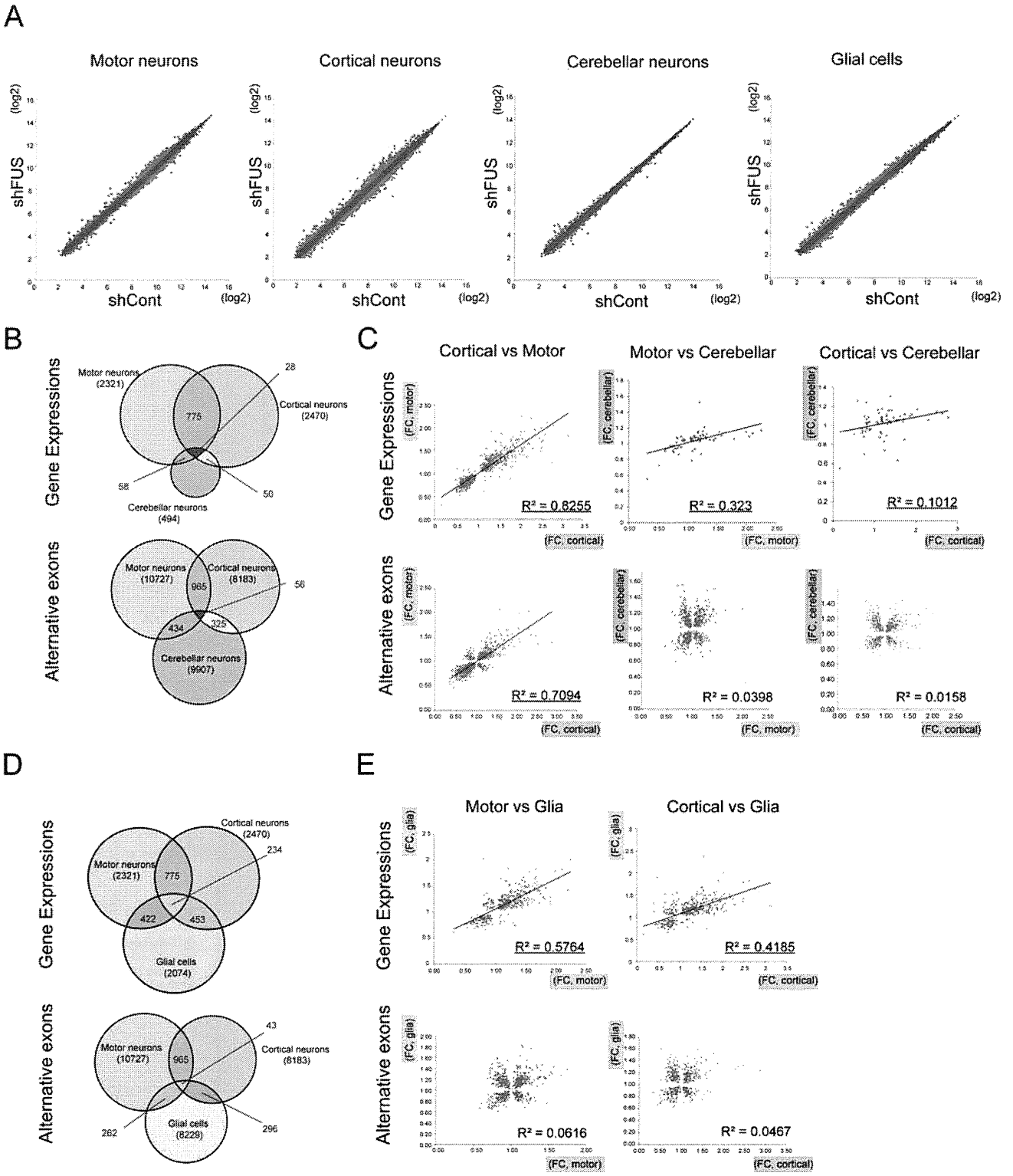

Figure 2 | Comparison of gene expression and exon splicing profiles among different cell lineages from the central nervous system after *Fus* knockdown. (A) Scatter plot analysis of gene expression using shCont and shFUS in different primary cells from the central nervous system. Genes whose expression levels changed by more than 1.3-fold after Fus-silencing with shFUS1 are indicated in red. (B) The profiles of gene expression and alternative splicing events were compared among the three different primary neurons. Venn diagrams indicate overlap in genes (*top*) and exons (*bottom*) whose expression levels are uniquely or concordantly regulated by FUS among motor, cortical, and cerebellar neurons ($p < 0.1$, by t-test). (C) The fold-changes in overlapped genes filtered by the t-test ($p < 0.1$) were plotted for primary motor, cortical, and cerebellar neurons. Scatter plots of fold-changes in gene expression levels (*top*) and alternative splicing events (*bottom*) after *Fus* knockdown. The R^2 value was calculated for genes and exons with t-test p values $<$ 0.1. (D) As in Fig. 2B, the profiles of gene expression and alternative splicing events in glial cells were compared with those of motor and cortical neurons. Venn diagrams indicate overlap in genes (*top*) and exons (*bottom*) whose expression levels are uniquely or concordantly regulated by FUS among motor, cortical, and glial cells ($p < 0.1$, by t-test). (E) Scatter plots of fold-changes in gene expression levels (*top*) and alternative splicing events (*bottom*) after *Fus* knockdown. The R^2 value was calculated for genes and exons with t-test p values < 0.1.

neurons (R^2 = 0.58 and 0.42, respectively). On the other hand, comparisons of exon splicing profiles did not show a significant correlation between motor neurons and glial cells, and cortical neurons and glial cells (R^2 < 0.1, each, Fig. 2E). Thus, FUS regulates the expression levels and alternative splicing of the largest number of shared genes between cortical and motor neurons. Similarly, though less concordantly, FUS regulates the expression levels of the same genes among the cortical/motor, cerebellar, and glial cells, but not alternative splicing of these cells.

Characterization of genes with altered gene expression and spliced alternative exon regulated by FUS in different cell lineages of the CNS. We also analyzed Gene Ontology (GO) terms of genes shown in the Venn diagrams using DAVID 6.7[21,22]. The GO terms of genes regulated by FUS in primary motor neurons were mainly those involved in signaling cascades and metabolic processes that were similar to those in primary cortical neurons (Table 1). The GO terms of those in glial cells are mainly involved in the regulation of the immune system. The GO terms of those in cerebellar neurons were not available since the number of differentially expressed genes was too small. The GO terms of genes involved in FUS-related regulation of alternative splicing events in both motor and cortical neurons were mainly involved in various neuronal functions such as synapse, nerve impulse, and neuronal projection. In contrast, none of

Table 1 | Gene Ontology terms for FUS-associated genes in each primary cell type

	GO ID	Term	*P* value
Gene expression			
Motor neurons			
	GO:0008104	protein localization	0.002392
	GO:0006796	phosphate metabolic process	0.002963
	GO:0006793	phosphorus metabolic process	0.002963
	GO:0015031	protein transport	0.006112
	GO:0045184	establishment of protein localization	0.006463
	GO:0016310	phosphorylation	0.012273
	GO:0006468	protein amino acid phosphorylation	0.014793
Cortical neurons			
	GO:0019637	organophosphate metabolic process	3.68E-04
	GO:0006644	phospholipid metabolic process	4.89E-04
	GO:0016055	Wnt receptor signaling pathway	5.21E-04
	GO:0009100	glycoprotein metabolic process	5.30E-04
	GO:0007264	small GTPase mediated signal transduction	5.91E-04
	GO:0006650	glycerophospholipid metabolic process	8.42E-04
	GO:0007242	intracellular signaling cascade	0.001227
Glial cells			
	GO:0009615	response to virus	1.68E-08
	GO:0006955	immune response	1.18E-07
	GO:0048525	negative regulation of viral reproduction	0.012033
	GO:0006952	defense response	0.01839
	GO:0045087	innate immune response	0.026843
	GO:0008653	lipopolysaccharide metabolic process	0.035673
	GO:0050792	regulation of viral reproduction	0.047282
Alternative splicing			
Motor neurons			
	GO:0006836	neurotransmitter transport	0.003894
	GO:0007268	synaptic transmission	0.018152
	GO:0032940	secretion by cell	0.019717
	GO:0046903	secretion	0.027201
	GO:0019226	transmission of nerve impulse	0.028352
	GO:0007269	neurotransmitter secretion	0.041581
	GO:0007267	cell-cell signaling	0.044736
Cortical neurons			
	GO:0045202	synapse	6.85E-07
	GO:0042995	cell projection	2.54E-06
	GO:0043005	neuron projection	2.29E-05
	GO:0005856	cytoskeleton	1.73E-04
	GO:0005886	plasma membrane	1.88E-04
	GO:0043232	intracellular non-membrane-bounded organelle	2.07E-04
	GO:0043228	non-membrane-bounded organelle	2.07E-04
Glial cells			
	GO:0030097	hemopoiesis	0.006476
	GO:0048534	hemopoietic or lymphoid organ development	0.008832
	GO:0002520	immune system development	0.010084
	GO:0030098	lymphocyte differentiation	0.013204
	GO:0002521	leukocyte differentiation	0.019998
	GO:0007517	muscle organ development	0.029812
	GO:0046649	lymphocyte activation	0.034644
Cerebellar neurons			
	GO:0051301	cell division	0.006634
	GO:0046632	alpha-beta T cell differentiation	0.026253
	GO:0046631	alpha-beta T cell activation	0.031696

the neuronal function terms emerged in the list of alternative splicing events in cerebellar neurons. Alternative splicing events in glial cells were mostly categorized into immunohematological functions (Table 1).

Supplementary Table S3 lists the top 10 genes that were differentially expressed in Fus-silenced motor neurons, together with the fold-change values in cortical neurons, glial cells, and cerebellar neurons. Similar to the global profile comparison shown in Fig. 2, the expression patterns of genes in the three different primary cells were similar except for cerebellar neurons, whose profile was less altered by Fus-depletion than other cell types.

After filtering exons with genes that were differentially expressed by both shFUS1 and shFUS2 with t-test p value of ≤ 0.1 and with fold-changes ≥ 1.3-fold in each primary cell, we categorized alternative splicing exons into category "A" to "E". In total, 44 exons were validated by RT-PCR and shown in Table 2, Fig. 3A–C, and Supplementary Fig. S3A–E. Alternative splicing exons A were specific to primary cortical neurons and primary motor neurons; B, specific to primary motor neurons; C, specific to primary cortical neurons; D, specific to primary glial cells, E, were common among primary motor neurons, cortical neurons, glial cells and/or cerebellar neurons.

We identified 18 alternative splicing events that were motor- and cortical neuron-specific, including *Mapt*, *Dlgap4*, and *Snap25* (Fig. 3A). All the validated splicing events that were motor- and cortical neuron-specific are shown in Supplementary Fig. S3A. We observed motor-neuron-specific alternative splicing events in *Synj1*, *Scn8a*, and *Rims1* (Fig. 3B). We also identified several alternative spliced events that were differentially expressed in Fus-silenced cortical neurons. Fig. 3C shows representative cortical-neuron-specific alternative splicing events in *Kcnip*, *Stxbp1*, and *Fmr1*. All the validated events are shown in Supplementary Fig. S3C. Furthermore, Glial-cell-specific alternative splicing events were seen in *Sgce*, *Wdr35*, and *Fip1l1* (Supplementary Fig. S3C). Exons in *Fxr1* and *Tsc22d2* were alternatively spliced in all primary cell types. *Map4* exon14 inclusion was also observed in primary cortical neurons,

Table 2 | List of validated FUS-regulated cell-type specific alternative splicing events

gene symbol	alternative splicing	motor neurons	cortical neurons	glial cells	cerebellar neurons	group
Mapt	Ex10 inclusion	✓	✓	-	-	A
Dlgap1	Ex10 inclusion	✓	✓	-	-	A
Snap25	Alternative exon (Ex5)	✓	✓	-	-	A
Anks1b	Ex7 inclusion	✓	✓	-	-	A
Brcc3	3′UTR elongation	✓	✓	-	-	A
Tia1	Ex5 inclusion	✓	✓	-	-	A
Caskin1	Ex15-16 skipping	✓	✓	-	-	A
Clec16a	Ex10 shortening	✓	✓	-	-	A
Elmo2	Ex10 skipping	✓	✓	-	-	A
Erc2	Ex12 skipping	✓	✓	-	-	A
Fkbp15	Ex19 elongation	✓	✓	-	-	A
Grm5	Ex8 inclusion	✓	✓	-	-	A
Lrrc7	Ex23 skipping	✓	✓	-	-	A
Pdzd4	Ex2-3 skipping	✓	✓	-	-	A
Smarca1	Ex3 alternative exon	✓	✓	-	-	A
Tcerg1l	Ex7 elongation	✓	✓	-	-	A
Xpr1	Ex13 elongation	✓	✓	-	-	A
Anks1	Ex24 skipping	✓	✓	-	-	A
Synj1	Ex27 inclusin	✓	-	-	-	B
Rims1	Alternative 3′-UTR	✓	-	-	-	B
Scn8a	Alternative exon (Ex4)	✓	-	-	-	B
Stxbp1	Ex19 skipping	-	✓	-	-	C
Kcnip1	Ex2 skipping	-	✓	-	-	C
Fmr1	Ex12 inclusion	-	✓	-	-	C
Abi1	Ex8 skipping	-	✓	-	-	C
CamK2a	Ex14 skipping	-	✓	-	-	C
Cttn	Ex11 skipping	-	✓	-	-	C
Grip1	Ex10 inclusion	-	✓	-	-	C
Nav2	Ex5 inclusion	-	✓	-	-	C
Neo1	Ex26 skipping	-	✓	-	-	C
Ndrg3	Ex16 skipping	-	✓	-	-	C
Rapgef4	Ex7 inclusion	-	✓	-	-	C
Sh3kbp1	Ex6-7 inclusion	-	✓	-	-	C
Slc1a2	Ex11 skipping	-	✓	-	-	C
Ttll5	Ex33 skipping	-	✓	-	-	C
Zhx1	Ex3 skipping	-	✓	-	-	C
Braf	Ex12 skipping	-	✓	-	-	C
Wdr35	Ex11 inclusion	-	-	✓	-	D
Sgce	Ex2 inclusion	-	-	✓	-	D
Fip1l1	Ex9 inclusion	-	-	✓	-	D
Fxr1	Ex15-16 inclusion	✓	✓	✓	✓	E
Tsc22d2	Ex2 inclusion	✓	✓	✓	✓	E
Map4	Ex14 inclusion	✓	✓	✓	-	E
Ntng1	Ex7 inclusion	✓	✓	-	✓	E

✓:changed significantly with Fus silencing.
A: specific to primary cortical neurons and primary motor neurons; B, specific to primary motor neurons; C, specific to primary cortical neurons; D, specific to primary glial cells, E, common among primary motor neurons, cortical neurons, glial cells and/or cerebellar neurons.

Figure 3 | Validation of representative altered splicing events in different cell lineages from the central nervous system after *Fus-silencing*. (A–C) Three representative alternative splicing events regulated by Fus are shown in each category: (A) both motor and cortical neuron-specific, (B) motor neuron-specific, and (C) cortical neuron-specific. All the validation of altered splicing events including category D and E, are shown in Supplementary Fig. S3. The top panels represent schematic splicing changes mediated by FUS. shCont and shFus resulted in splicing events shown in the top and bottom rows, respectively. The second panels show representative RT-PCR of the indicated exons in primary motor neurons. Similarly, the third, fourth, and fifth panels show representative RT-PCR of the indicated exons in primary cortical neurons, primary glial cells, and primary cerebellar neurons, respectively. The experiments were repeated four times using four independent sets of samples. The results of densitometric quantification of RT-PCR are shown in bar graphs (n = 4; mean ± SD). *$p < 0.05$, between shCont and shFUS (by Student's t-test).

motor neurons, and glial cells; but not in cerebellar neurons (Supplementary Fig. S3D).

Interestingly, we also identified many neurological disease-associated genes among the profiles of gene expression and alternative splicing events. We list such representative genes in Table 3.

The protein levels of representative genes with altered spliced events and gene expression were validated by immunoblot in all four primary cells in the CNS (Fig. 4). The expression of 4-repeat Tau (RD4) which corresponds to the exon10 (+) isoform of *Mapt* gene was increased by shFUS in primary cortical neurons but was undetectable in motor neurons. On the other hand, the expression of 3-repeat Tau (RD3) which corresponds to the exon10 (-) isoform was decreased in primary cortical and motor neurons. The 89kD form of Braf protein encoded by the exon12 (+) variant of *Braf* gene was decreased in Fus-silenced primary cortical neurons. The protein expression level of Syntaxin-1A was upregulated in Fus-silenced cortical and motor neurons as observed in its mRNA levels.

Direct binding of FUS to target mRNA was not tisseue-type specific in CNS. To investigate the direct binding of FUS to mRNA of the genes and exons with altered expression, RNA immunoprecipitation (RIP) using differenet tissues of CNS was performed. We prepared the spinal cord (E13), the cerebrum (E15), and the cerebellum (E15) from the mouse embryos, and FUS protein was immunoprecipitated from each tissue (Fig. 5A). FUS-associated mRNA levels were evaluated by RT-PCR using specific primers for *Mapt*, *Dlgap1*, and *Stxbp1*, of which alternative splicing events were regulated by FUS. Primers for *Gapdh* and intergenic region were used as negative controls. The RIP results showed that the interaction levels between FUS and mRNA of *Mapt*, *Dlgap1*, and *Stxbp1* among three different CNS tissues were comparable, whereas these three genes showed cell-type specific splicing patterns in Fig 3 (Fig. 5B). There was no apparent binding of FUS to *Gapdh* mRNA or intergenic region (Fig. 5B). We next analyzed position dependence of FUS-binding to splicing targets and their effects on alternative splicing through comprehensive analysis of the exon array using primary glial cells and HITS-CLIP of mouse brain (Fig. 5C–D). We analyzed the positions of CLIP-tags of 121 FUS-responsive exons (29 exon skipped and 92 exon included by shRNA) that were filtered by t-test p value ≤ 0.1 and fold-change of ≤ 0.67 or ≥ 1.5 for shFUS1. We combined these exons into a single composite pre-mRNA and prepared integrated RNA maps from our HITS-CLIP reads mapped to the corresponding genomic regions, as described in more detail previously[23–25]. The analysis showed that scattered FUS binding sites mainly around the alternatively spliced exons. Conspicuous binding of FUS was observed at ~500 nt upstream of the 3′ end of the downstream intron in skipped exons (arrows in Fig. 5C). This finding was similar to the complexity map of primary cortical neurons that was reported previously by our group (Fig. 5D)[20].

Discussion

In the present study, we determined the gene expression profiles and alternative splicing events in four different primary cells of the CNS, with silenced *Fus* induced by lentivirus encoding shRNA against *Fus*. By comparing the gene expression profiles of the four primary cells, we found that the genes altered by Fus-silencing were fewer in cerebellar neurons than in the other three cell types, although the innate gene expression profiles of motor, cortical and cerebellar neurons were similar. These findings suggest that gene expression profile reflects cellular response affected by Fus-silencing in each cell type, given that ALS/FTLD-relevant cell types showed more alterations than non- ALS/FTLD-relevant cell type. On the other hand, the profiles of alternative splicing events were only similar in motor and cortical neurons. Alternative splicing events in these two types of neurons were far different from glial cells and cerebellar neurons, suggesting that alternative splicing events are uniquely fine-tuned in a cell-specific manner (Fig. 2). Alternative splicing contributed to brain development in mammals during the evolution process[26,27]. In the adult human, the brain expresses more alternatively spliced transcripts than any other tissues[28], and the majority of splicing events are regulated in a tissue-specific manner[29]. Our finding that FUS-regulated alternative splicing events were more region- and cell-type-specific than those of gene expression suggests that the profiles of alternative splicing events may reflect direct phenomenon caused by Fus-depletion whereas those of gene expression include both indirect phenomenon as well as direct suppressive effects on transcription by binding to promoter antisense transcripts[20]. Indeed, we observed more frequent FUS-tagged sites on genes with altered spliced alternative exons than genes with altered gene expression (Supplementary Fig. S4). In this context, the alternative splicing events regulated by FUS could explain the cell vulnerability in ALS/FTLD associated with FUS, whereas the gene expression regulated by FUS could represent the size of cellular impact in FUS-associated ALS/FTLD. The fact that cell death broadly occurs in the cerebral cortex but not in the cerebellum and that cell death occurs only in neurons but not in glial cells in ALS/FTLD also supports this notion[30,31]. Although we found cell-type-specific profiles of FUS-regulated alternative splicing events, the RIP experiments showed that direct interaction between FUS and target RNA was comparable in different CNS tissues. The complexity map showed similar patterns for FUS-binding positions around the alternatively spliced exons in cortical neurons and glial cells. These findings indicate that FUS binding to mRNA is not dependent on cell/tissue type. Instead, other molecules that associate with FUS in the spliceosome are likely to dictate cell/tissue type-specificity of FUS-mediated alternative splicing events. FUS protein-interaction analysis may provide more detail information about cell specific machinery of FUS on alternative RNA splicing.

Table 3 | List of FUS-regulated genes/exons in various neurological disease

Gene	Effect by Fus-silencing	Cell type	Neurological Disease	Neuronal Function
Mapt	Ex10 inclusion	motor/cortical	FTLD	microtuble stabilization
Fmr1	Ex12 inclusion	cortical	Fragile X	Translation repressor
Fxr1	Ex15−16 inclusion	all	Fragile X	RNA-binding protein
Stx1a	upregulation	motor/cortical	Williams-Beuren syndrome	Part of the SNARE core complex
Snap25	Ex5 alternative exon	motor/cortical		Part of the SNARE core complex
Stxbp1	Ex19 skipping	cortical	EIEE4	binding to syntaxins
Camk2a	Ex14 skipping	cortical	Alzheimer's disease	LTP
Scn8a	Ex4 alternative exon	motor	EIEE13	sodium channel
Sgce	Ex2 inclusion	glial	Myoclonus dystonia	dystrophin-glycoprotein complex
Fktn	downregulation	all	Congenital muscular dystrophy	glycosyltransferase

EIEE4: epileptic encephalopathy early infantile type 4.
EIEE13: epileptic encephalopathy early infantile type 13.

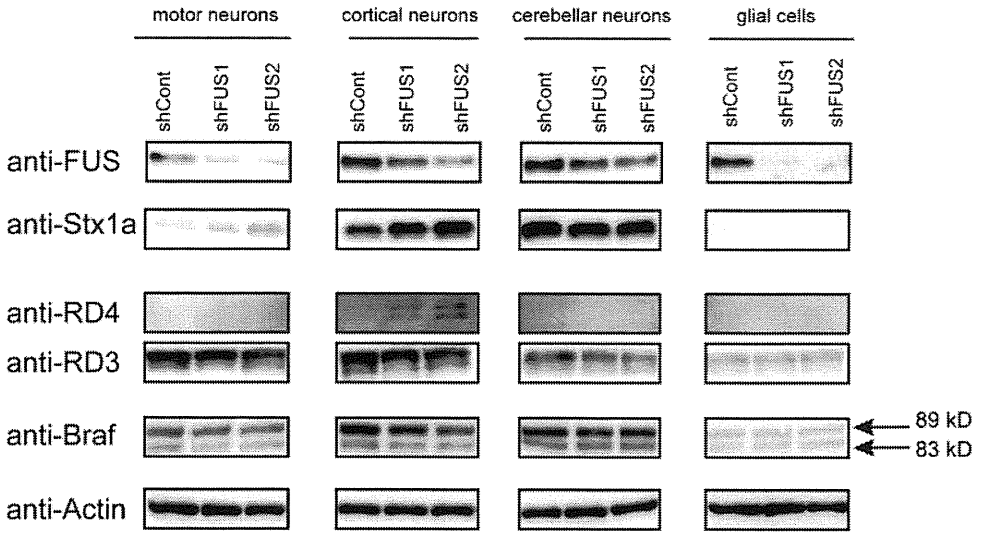

Figure 4 | Protein expressions of genes with altered splicing events and gene expression in different cell lineages from the central nervous system after *Fus*-silencing. Protein levels of representative genes with altered splicing events (Tau and Braf) and gene expression (Syntaxin-1A) were evaluated in different primary cells in the CNS with Fus-silencing. Expression levels of FUS, Syntaxin-1A (Stx1a), 3-repeat Tau (RD3), 4-repeat Tau (4RD), Braf, and actin were measured by immunoblot.

The results showed concordant regulation of many alternative splicing events by FUS in both motor and cortical neurons, which underscores the notion that FUS-mediated ALS and FTLD could be considered the same disease entity based on clinicopathological and genetic findings[7,32]. The cell-type specific transcriptome profiles we established were embryonic; however many of identified FUS-mediated splicing events were likely to be seen in adult tissues. Indeed, 34% (15/44) of alternative splicing events in Table2 were also seen in the list of another report[33] using adult mouse brain with Fus-silencing (data not shown). Among them, *Mapt* is the most notable gene whose splicing was affected by Fus-depletion (Fig. 3A and Table 2). The inclusion exon 10 yields 4-repeat Tau (RD4), whereas skipping of exon10 generates 3-repeat Tau (RD3). We reported previously the increase of exon 10 inclusion in *Mapt* in Fus-silenced primary cortical neurons, a finding also reported by several other groups[20,33–35]. In this study, we also found the increase of exon 10 inlusion in primary motor neurons, although the protein level of RD4 was only dectable in cortical neurons. In this regard, it is intriguing that previous studies reported the presence of high RD4/RD3 ratio in various neurodegenerative disorders, including FTLD[36,37]. However, little is known about the involvement of Tau pathology in motor neuron degeneration in ALS. Further studies are necessary to clarify the association between the FUS-Tau pathway and pathogenesis of ALS and FTLD.

As described above, the entire profiles of alternative splicing events in motor and cortical neurons were almost identical. Nonetheless, we identified only motor neuron- or cortical neuron-specific alternative splicing events with close observation of region- and cell-type specific profiles of alternative splicing. Those splicing events may potentially represent differences in cell fate in each clinical subtype of ALS/FTLD. We identified some channel-associated genes, such as *Synj1*, *Scn8a*, and *Rims1* as motor neuron-specific alternative splicing targets regulated by FUS (Fig. 3B and Table 2), indicating that synaptic dysfunction provoked by Fus-silencing seems to be one of causes of motor neuron degeneration.

On the other hand, cortical neuron-specific alternative exons might affect cerebral neurons, leading to cortex pathology in FTLD. *Stxbp1* is the causative gene for epileptic encephalopathy early infantile type 4 (EIEE4)[38] and participates in the regulation of synaptic vesicle docking and fusion by associating with the SNARE complex, which is essential for fusion of opposing cellular membranes necessary for neurotransmission[39]. It is noteworthy that two other SNARE complex components; Syntaxin-1A and Snap25, were also identified as FUS-regulated gene and alternative exon, respectively (Fig. 3C and Table 2). Fmr1 is essential for normal cognitive development and its mutation can lead to fragile X syndrome characterized by mental retardation, autism, Parkinson's disease, and other cognitive deficits[40]. The other fragile X syndrome-related gene, *Fxr1*, is also included among the list of alternative exons in which *Fxr1* exon 16 is skipped by Fus-silencing in all cell types (Supplementary Fig. S3D and Table 3).

Involvement of glial cells, such as astrocytes and microglia, likely modifies and exaggerates the ALS/FTLD disease process. Although it is not clear whether non-cell autonomous mechanism is also relevant to FUS-associated ALS/FTLD, we showed here that primary glial cells showed more altered differential genes by Fus-silencing than cerebellar neurons (Fig. 2A), suggesting that knock-down of FUS gene could have certain impact on cellular homeostasis of glial cells, in addition to motor and cortical neurons.

Our global analysis also identified several genes relevant to various neurological diseases (Table 3). The alteration of gene expression and/or alternative splicing of these genes may have a large impact on neuronal function. It is unlikely that only one of these genes or exons is solely responsible for neurodegeneration in ALS/FTLD. FUS silencing would have a partial effect instead of total loss of function by altering isoforms or down/up regulation of these genes; therefore, it is possible that accumulation of altered genes affected by FUS-depletion could cause neurodegeneration after reaching a critical threshold level even when the individual alternative splicing event and gene expression are not critical by themselves. Investigation of FUS-targeting molecules, especially those relevant to neurological diseases may provide mechanistic insights into selective neuronal degeneration in FUS-associated ALS/FTLD.

Methods

Primary cells from the central nervous system. Primary motor neurons were harvested from the spinal cords of C57BL/6 mouse embryos at embryonic (E) day 13. Primary cortical neurons and primary glial cells were obtained from the cerebri of C57BL/6 mice at E15. Primary cerebellar neurons were obtained from cerebelli of C57BL/6 mice at E15. The procedure for culture of each primary cell and lentivirus infection are described in the online supplementary information. All animal experiments were performed in accordance with the National Institutes of Health Guide for the Care and Use of Laboratory Animals and under the approval of the Nagoya University Animal Experiment Committee (Nagoya, Japan).

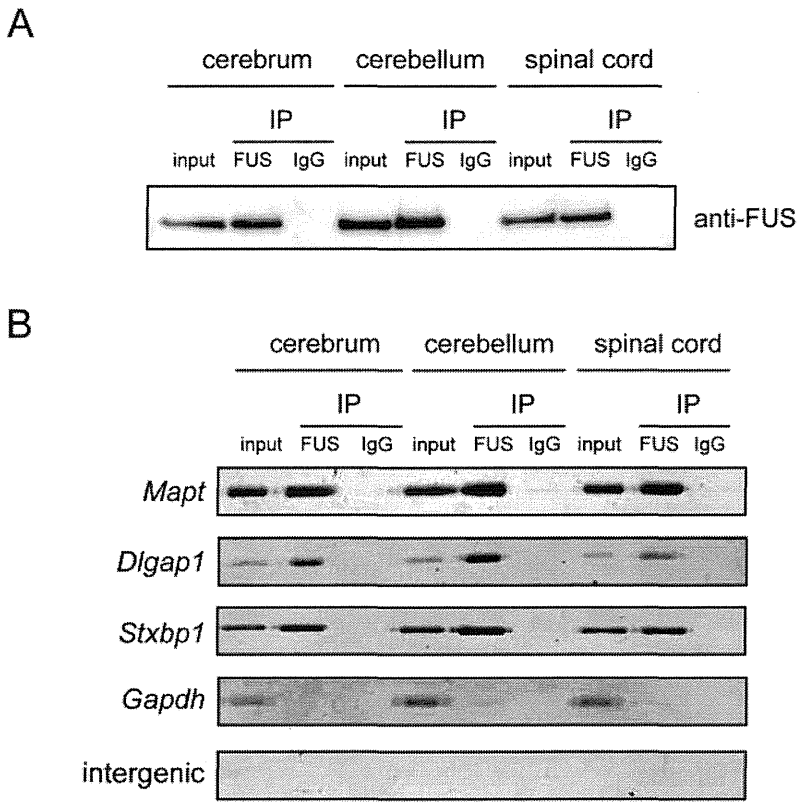

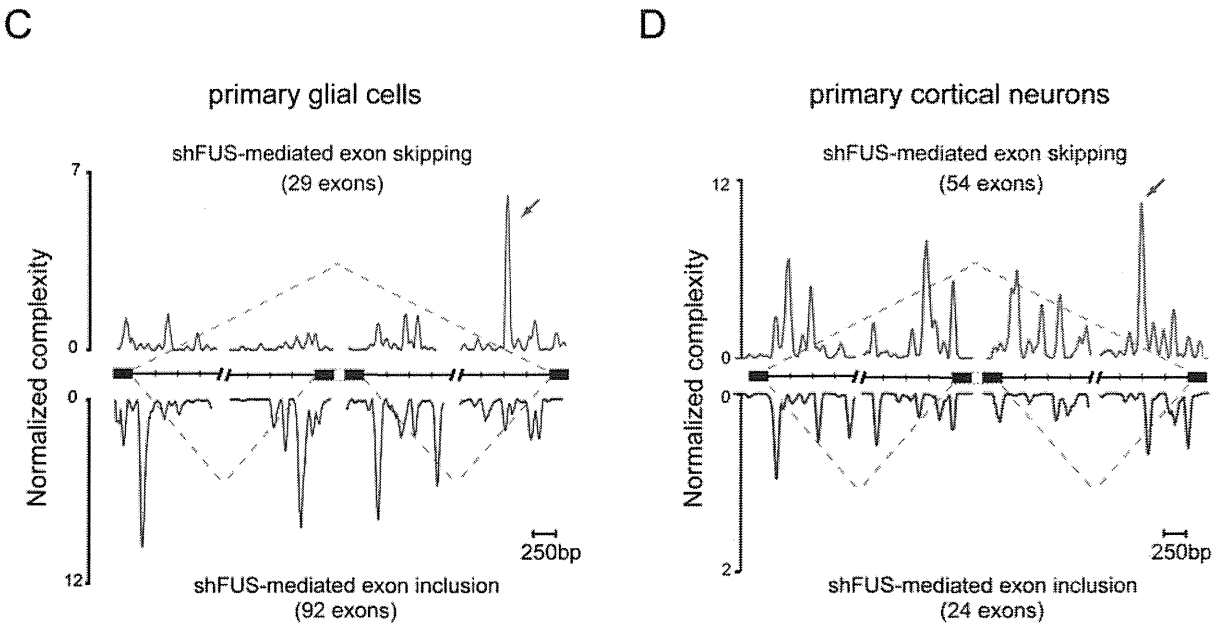

Figure 5 | The binding of FUS to mRNA is not tissue and cell type specific in the CNS. (A–B) RNA immunoprecipitation (RIP) was performed to detect the interaction between FUS and mRNA of genes with altered splicing events using mouse cerebrum, cerebellum, and spinal cord. (A) Anti-FUS immunoblot of 1% input, FUS-IP, and control IP (IgG) from mouse cerebrum, cerebellum, and spinal cord at E15 embryos was shown. (B) FUS-associated RNA was reverse transcribed and evaluated by semi-quantative PCR with specific primers for three representative FUS-target genes with altered alternative splicing events, *Mapt*, *Dlgap1*, and *Stxbp1*. Primers for *Gapdh* and intergenic region (intergenic) were used as controls. (C–D) We compared normalized complexity map of FUS-dependent splice sites of primary glial cells and cortical neurons. shFUS-mediated alternative splicing events in primary glial cells (C) and primary cortical neurons (D) are compiled. Blue arrows point to conspicuous peaks at ~500 nt upstream of the 3′ end of the downstream intron. The complexity map of primary cortical neuron (D) is identical to that shown in the Supporting Information/Fig. S3 in our previous report[20], which is shown for comparison with that of primary glial cells (C).

Lentivirus. We designed two different shRNAs against mouse *Fus* as well as a control shRNA. The targeted sequences were 5′-GCAACAAAGCTACGGACAA-3′ for shRNA/FUS1 (shFUS1); 5′-GAGTGGAGGTTATGGTCAA-3′for shRNA/FUS2 (shFUS2); and 5′-AATTCTCCGAACGTGTCACGT-3′ for shRNA/control (shCont). These were cloned into a lentiviral shRNA vector (pLenti-RNAi-X2 puro DEST, w16-1, a kind gift from Dr. Eric Campeau at Resverlogix Corp., Calgary, Alberta, Canada). Lentivirus was prepared using the protocol described by Campeau et al[41]. Briefly, lentiviral particles were produced in HEK293T cells by transfection using Lipofectamine 2000 (Invitrogen, Carlsbad, CA). The lentivirus-containing supernatant was collected at 48 hours after transfection, and stored at −80°C. Lentivirus titer was measured using NucleoSpin RNA Virus kit (Clontech, Mountain View, CA).

Microarray analysis. Total RNA was extracted from primary motor neurons, cortical neurons, cerebellar neurons, and glial cells by the RNeasy Mini kit (Qiagen, Hilden, Germany). We confirmed that the RNA integrity numbers (RIN) were all above 7.0. cDNA fragments were synthesized and labeled from 100 ng of total RNA using the GeneChip WT cDNA Synthesis Kit (Ambion, Austin, TX). Hybridization and signal acquisition of the GeneChip Mouse Exon 1.0 ST exon array (Affymetrix, Santa Clara, CA) were performed according to the instructions provided by the manufacturer. Each array experiment was performed in triplicate. The exon-level and gene-level signal intensities were normalized by the RMA and iterPLIER methods, respectively, using the Expression Console 1.1.2 (Affymetrix). We followed the gene annotation of the ENSEMBL version e!61, which is based on the mouse genome assembly NCBI build 37.1/mm[9]. All microarray data were registered in the Gene Expression Omnibus with accession number GSE36153 for cortical neurons, GSE42421 for motor neurons, glial cells, and cerebellar neurons.

The principal component analysis of innate gene profiles in each cell type was conducted using the GeneSpring software (Agilent Technologies). For each cell type, the gene-level signal intensities of three controls treated with shCont were compared with those of three samples treated either with shFUS1 or shFUS2, using the Student's t-test. The gene expression profiles for each cell-type were established with or without statistical filtration of the t-test p value ≤ 0.1. We also obtained alternative splicing profiles by filtering the exon-level signal intensities of the probe sets on internal exons with t-test p value ≤ 0.1. Comparison analysis of the profiles was completed using shCont and shFUS1 subsets for each cell-type profile.

RT-PCR for alternative splicing analysis. Total RNA was isolated from cells using RNeasy Mini Kit (Qiagen, Hilden, Germany) followed by treatment with DNaseI (Qiagen). cDNA was synthesized from 1 μg of total RNA with the Oligo-dT primer (Promega, Madison, WI). The primers for each candidate exon were designed using Primer3 software (http://frodo.wi.mit.edu/primer3/input.htm). The sequences of primers are shown in Supplementary Table S4. Semi-quantitative RT-PCR was performed using Ex Taq (Takara Bio Inc, Otsu, Japan) at 25–30 cycles at 98°C for 10 sec, 60°C for 30 sec, and 72°C for 1 min. PCR products was electrophoresed on 15% acrylamide gel and stained with ethidium bromide. The intensity of each band was measured by Multi Gage software (Fujifilm, Tokyo).

Immunoblot. Cells were lysed in TNE buffer containing protease inhibitors for 15 min on ice. The lysates were then cleared by centrifuging the cells at 13,000 g for 15 min at 4°C. Lysates were normalized for total protein (10 μg per lane), separated using a 4%–20% linear gradient SDS-PAGE and electroblotted. For immunoblot, we used anti-FUS antibodies (A300-293A, Bethyl Laboratories, Montgomery, TX and 4H11, Santa Cruz Biotechnology, Santa Cruz, CA), anti-Syntaxin-1A antibody (abcam, Cambridge, MA), anti-RD3 antibody (Millipore, Billerica, MA), anti-RD4 antibody (Millipore), anti-Braf antibody (Thermo Scientific, South Logan, UT), and anti-actin antibody (Sigma, St. Louis, MO).

RNA imunoprecipitation (RIP). Extracts were taken from mouse cerebrum, cerebellum, and spinal cord at E15, normalized for total protein (1.6 mg), and applied for RIP using anti-FUS antibody (A300-293A, Bethyl Laboratories) and RIP-Assay Kit (MBL, Nagoya Japan). Immunoprecipitation using rabbit IgG was used as a control. Semi-quantitative RT-PCR was performed using Ex Taq (Takara Bio Inc, Otsu, Japan) and random primers at 22–25 cycles at 98°C for 10 sec, 60°C for 30 sec, and 72°C for 1 min. Based on the HITS-CLIP analysis information in our previous study, we designed primers for *Mapt* at exon6, *Dlgap1* at exon11, and *Stxbp1* at exon20, respectively. Primers for *Gapdh* and an intergenic region were used as controls.

Bioinformatics analysis. The detail was described in Supplementary experimental procedures.

1. Rothstein, J. D. Current hypotheses for the underlying biology of amyotrophic lateral sclerosis. *Ann Neurol* **65 Suppl 1**, S3–9 (2009).
2. Saxena, S. & Caroni, P. Selective neuronal vulnerability in neurodegenerative diseases: from stressor thresholds to degeneration. *Neuron* **71**, 35–48 (2011).
3. Strong, M. J. & Volkening, K. TDP-43 and FUS/TLS: sending a complex message about messenger RNA in amyotrophic lateral sclerosis? *FEBS J* **278**, 3569–77 (2011).
4. Lagier-Tourenne, C. & Cleveland, D. W. Rethinking ALS: the FUS about TDP-43. *Cell* **136**, 1001–4 (2009).
5. Munoz, D. G. *et al.* FUS pathology in basophilic inclusion body disease. *Acta Neuropathol* **118**, 617–27 (2009).
6. Neumann, M. *et al.* A new subtype of frontotemporal lobar degeneration with FUS pathology. *Brain* **132**, 2922–31 (2009).
7. Van Langenhove, T., van der Zee, J. & Van Broeckhoven, C. The molecular basis of the frontotemporal lobar degeneration-amyotrophic lateral sclerosis spectrum. *Ann Med* **44**, 817–28 (2012).
8. Kwiatkowski, T. J., Jr. *et al.* Mutations in the FUS/TLS gene on chromosome 16 cause familial amyotrophic lateral sclerosis. *Science* **323**, 1205–8 (2009).
9. Vance, C. *et al.* Mutations in FUS, an RNA processing protein, cause familial amyotrophic lateral sclerosis type 6. *Science* **323**, 1208–11 (2009).
10. Deng, H. X. *et al.* FUS-immunoreactive inclusions are a common feature in sporadic and non-SOD1 familial amyotrophic lateral sclerosis. *Ann Neurol* **67**, 739–48 (2010).
11. Bosco, D. A. *et al.* Mutant FUS proteins that cause amyotrophic lateral sclerosis incorporate into stress granules. *Hum Mol Genet* **19**, 4160–75 (2010).
12. Dormann, D. *et al.* ALS-associated fused in sarcoma (FUS) mutations disrupt Transportin-mediated nuclear import. *EMBO J* **29**, 2841–57 (2010).
13. Ito, D., Seki, M., Tsunoda, Y., Uchiyama, H. & Suzuki, N. Nuclear transport impairment of amyotrophic lateral sclerosis-linked mutations in FUS/TLS. *Ann Neurol* **69**, 152–62 (2011).
14. Kino, Y. *et al.* Intracellular localization and splicing regulation of FUS/TLS are variably affected by amyotrophic lateral sclerosis-linked mutations. *Nucleic Acids Res* **39**, 2781–98 (2011).
15. Wang, J. W., Brent, J. R., Tomlinson, A., Shneider, N. A. & McCabe, B. D. The ALS-associated proteins FUS and TDP-43 function together to affect Drosophila locomotion and life span. *J Clin Invest* **121**, 4118–26 (2011).
16. Kabashi, E. *et al.* FUS and TARDBP but not SOD1 interact in genetic models of amyotrophic lateral sclerosis. *PLoS Genet* **7**, e1002214 (2011).
17. Boillee, S. *et al.* Onset and progression in inherited ALS determined by motor neurons and microglia. *Science* **312**, 1389–92 (2006).
18. Yamanaka, K. *et al.* Mutant SOD1 in cell types other than motor neurons and oligodendrocytes accelerates onset of disease in ALS mice. *Proc Natl Acad Sci U S A* **105**, 7594–9 (2008).
19. Yamanaka, K. *et al.* Astrocytes as determinants of disease progression in inherited amyotrophic lateral sclerosis. *Nat Neurosci* **11**, 251–3 (2008).
20. Ishigaki, S. *et al.* Position-dependent FUS-RNA interactions regulate alternative splicing events and transcriptions. *Sci Rep* **2**, 529 (2012).
21. Huang da, W., Sherman, B. T. & Lempicki, R. A. Systematic and integrative analysis of large gene lists using DAVID bioinformatics resources. *Nat Protoc* **4**, 44–57 (2009).
22. Dennis, G., Jr. *et al.* DAVID: Database for Annotation, Visualization, and Integrated Discovery. *Genome Biol* **4**, P3 (2003).
23. Licatalosi, D. D. *et al.* HITS-CLIP yields genome-wide insights into brain alternative RNA processing. *Nature* **456**, 464–9 (2008).
24. Masuda, A. *et al.* CUGBP1 and MBNL1 preferentially bind to 3′ UTRs and facilitate mRNA decay. *Sci Rep* **2**, 209 (2012).
25. Xue, Y. *et al.* Genome-wide analysis of PTB-RNA interactions reveals a strategy used by the general splicing repressor to modulate exon inclusion or skipping. *Mol Cell* **36**, 996–1006 (2009).
26. Keren, H., Lev-Maor, G. & Ast, G. Alternative splicing and evolution: diversification, exon definition and function. *Nat Rev Genet* **11**, 345–55 (2010).
27. Grabowski, P. Alternative splicing takes shape during neuronal development. *Curr Opin Genet Dev* **21**, 388–94 (2011).
28. Yeo, G., Holste, D., Kreiman, G. & Burge, C. B. Variation in alternative splicing across human tissues. *Genome Biol* **5**, R74 (2004).
29. Clark, T. A. *et al.* Discovery of tissue-specific exons using comprehensive human exon microarrays. *Genome Biol* **8**, R64 (2007).
30. Geser, F. *et al.* Evidence of multisystem disorder in whole-brain map of pathological TDP-43 in amyotrophic lateral sclerosis. *Arch Neurol* **65**, 636–41 (2008).
31. Ravits, J. M. & La Spada, A. R. ALS motor phenotype heterogeneity, focality, and spread: deconstructing motor neuron degeneration. *Neurology* **73**, 805–11 (2009).
32. Da Cruz, S. & Cleveland, D. W. Understanding the role of TDP-43 and FUS/TLS in ALS and beyond. *Curr Opin Neurobiol* **21**, 904–19 (2011).
33. Lagier-Tourenne, C. *et al.* Divergent roles of ALS-linked proteins FUS/TLS and TDP-43 intersect in processing long pre-mRNAs. *Nat Neurosci* **15**, 1488–97 (2012).
34. Rogelj, B. *et al.* Widespread binding of FUS along nascent RNA regulates alternative splicing in the brain. *Sci Rep* **2**, 603 (2012).
35. Orozco, D. *et al.* Loss of fused in sarcoma (FUS) promotes pathological Tau splicing. *EMBO Rep* **13**, 759–64 (2012).
36. Yoshida, M. Cellular tau pathology and immunohistochemical study of tau isoforms in sporadic tauopathies. *Neuropathology* **26**, 457–470 (2006).
37. Hong, M. *et al.* Mutation-specific functional impairments in distinct tau isoforms of hereditary FTDP-17. *Science* **282**, 1914–7 (1998).
38. Saitsu, H. *et al.* De novo mutations in the gene encoding STXBP1 (MUNC18-1) cause early infantile epileptic encephalopathy. *Nat Genet* **40**, 782–8 (2008).
39. Tian, J. H., Das, S. & Sheng, Z. H. Ca2+-dependent phosphorylation of syntaxin-1A by the death-associated protein (DAP) kinase regulates its interaction with Munc18. *J Biol Chem* **278**, 26265–74 (2003).

40. Verheij, C. *et al.* Characterization and localization of the FMR-1 gene product associated with fragile X syndrome. *Nature* **363**, 722–4 (1993).
41. Campeau, E. *et al.* A versatile viral system for expression and depletion of proteins in mammalian cells. *PLoS One* **4**, e6529 (2009).

Acknowledgements

Part of this study represents the results of "Integrated Research on Neuropsychiatric Disorders" carried out under the Strategic Research Program for Brain Sciences by the Ministry of Education, Culture, Sports, Science and Technology of Japan. This work was also supported by Grants-in-Aid from the CREST/JST, MEXT, and MHLW of Japan.

Author contributions

Y.F., S.I., A.M., T.U. and Y.I. performed the experiments. Y.F., S.I., A.M., H.W., K.O. and G.S. analyzed the data. S.I., M.K., K.O. and G.S. prepared the manuscript. All authors reviewed the manuscript.

Additional information

Supplementary information accompanies this paper at http://www.nature.com/scientificreports

Accession codes Microarray data were uploaded to the Gene Expression Omnibus database: GSE36153 for cortical neurons, GSE42421 for motor neurons, glial cells, and cerebellar neurons.

Competing financial interests: The authors declare no competing financial interests.

How to cite this article: Fujioka, Y. *et al.* FUS-regulated region- and cell-type-specific transcriptome is associated with cell selectivity in ALS/FTLD. *Sci. Rep.* **3**, 2388; DOI:10.1038/srep02388 (2013).

ORIGINAL ARTICLE

Mutations in *COQ2* in Familial and Sporadic Multiple-System Atrophy

The Multiple-System Atrophy Research Collaboration

ABSTRACT

BACKGROUND

Multiple-system atrophy is an intractable neurodegenerative disease characterized by autonomic failure in addition to various combinations of parkinsonism, cerebellar ataxia, and pyramidal dysfunction. Although multiple-system atrophy is widely considered to be a nongenetic disorder, we previously identified multiplex families with this disease, which indicates the involvement of genetic components.

METHODS

In combination with linkage analysis, we performed whole-genome sequencing of a sample obtained from a member of a multiplex family in whom multiple-system atrophy had been diagnosed on autopsy. We also performed mutational analysis of samples from members of five other multiplex families and from a Japanese series (363 patients and two sets of controls, one of 520 persons and one of 2383 persons), a European series (223 patients and 315 controls), and a North American series (172 patients and 294 controls). On the basis of these analyses, we used a yeast complementation assay and measured enzyme activity of parahydroxybenzoate-polyprenyl transferase. This enzyme is encoded by the gene *COQ2* and is essential for the biosynthesis of coenzyme Q_{10}. Levels of coenzyme Q_{10} in lymphoblastoid cells and brain tissue were measured on high-performance liquid chromatography.

RESULTS

We identified a homozygous mutation (M78V-V343A/M78V-V343A) and compound heterozygous mutations (R337X/V343A) in *COQ2* in two multiplex families. Furthermore, we found that a common variant (V343A) and multiple rare variants in *COQ2*, all of which are functionally impaired, are associated with sporadic multiple-system atrophy. The V343A variant was exclusively observed in the Japanese population.

CONCLUSIONS

Functionally impaired variants of *COQ2* were associated with an increased risk of multiple-system atrophy in multiplex families and patients with sporadic disease, providing evidence of a role of impaired COQ2 activities in the pathogenesis of this disease. (Funded by the Japan Society for the Promotion of Science and others.)

The members of the Multiple-System Atrophy Research Collaboration are listed in the Appendix. Address reprint requests to Dr. Shoji Tsuji, Department of Neurology, University of Tokyo, 7-3-1 Hongo, Bunkyo-ku, Tokyo 113-8655, Japan, or at tsuji@m.u-tokyo.ac.jp.

This article was published on June 12, 2013, at NEJM.org.

N Engl J Med 2013;369:233-44.
DOI: 10.1056/NEJMoa1212115

Multiple-system atrophy is a progressive neurodegenerative disease that is clinically characterized by autonomic failure in addition to various combinations of parkinsonism, cerebellar ataxia, and pyramidal dysfunction. The term multiple-system atrophy was introduced in 1969 to encompass the disease entities of olivopontocerebellar ataxia, striatonigral degeneration, and the Shy–Drager syndrome, on the basis of neuropathological findings in these disorders.[1] Multiple-system atrophy is characterized by the development of cytoplasmic aggregates of α-synuclein, primarily in oligodendroglia.[2-7] However, the pathogenic mechanisms underlying this disease remain unknown, making it difficult to develop effective therapies.

The disorder is classified into two subtypes: subtype C, characterized predominantly by cerebellar ataxia, and subtype P, characterized predominantly by parkinsonism.[8] Among patients with multiple-system atrophy, subtype C has been reported to be more prevalent than subtype P in the Japanese population (65 to 67% vs. 33 to 35%),[9,10] whereas subtype P has been reported to be more prevalent than subtype C in Europe (63% vs. 34%)[11] and North America (60% vs. 13%, with 27% of cases unclassified).[12] Although multiple-system atrophy has been defined as a nongenetic disorder until recently, several multiplex families with the disease have been described, indicating that strong genetic factors confer susceptibility to the disease.[13-15]

METHODS

PATIENTS AND MULTIPLEX FAMILIES

Patients with multiple-system atrophy were enrolled in the study on the basis of research protocols that were approved by the institutional review board at each participating center. Written informed consent was obtained from all participants.

The diagnosis of multiple-system atrophy was made on the basis of the current consensus criteria for the disease.[8] Four Japanese families (Families 1 through 4, whose members have been described previously[13]) and two additional Japanese families (Family 8 and Family 12) were enrolled in this study (Fig. 1). In Family 1, the parents were first-degree cousins, which is consistent with autosomal recessive inheritance. The clinical features of these families are summarized in Table S1 in the Supplementary Appendix, available with the full text of this article at NEJM.org.

Autopsy findings for Participants II-4[13] and II-8 in Family 1 and Participant II-6 in Family 8 showed widespread and abundant cytoplasmic aggregates of α-synuclein, primarily in oligodendroglia, in association with neurodegeneration in striatonigral and olivopontocerebellar structures. These findings confirmed the diagnosis of multiple-system atrophy.

PATIENTS WITH SPORADIC DISEASE AND CONTROLS

As with the multiplex families, the diagnosis of sporadic multiple-system atrophy was made on the basis of the current consensus criteria.[8] A total of 363 patients with multiple-system atrophy and 520 controls were included in the Japanese series, 223 patients and 315 controls in the European series, and 172 patients and 294 controls in the North American series (persons of European or Hispanic descent living in North America) (Text S2 and Table S2 in the Supplementary Appendix). Ancestry was determined by self-report on a multiple-choice questionnaire. We also enrolled an independent series of 2383 Japanese controls.

ASSOCIATION WITH OTHER NEURODEGENERATIVE DISEASES

To determine the specificity of the association between variants in candidate genes and multiple-system atrophy, we enrolled 2728 Japanese patients with Alzheimer's disease, 659 with Parkinson's disease, and 634 with amyotrophic lateral sclerosis (ALS). Their demographic characteristics are provided in Text S2 in the Supplementary Appendix.

LINKAGE ANALYSIS AND WHOLE-GENOME SEQUENCING

We performed parametric and nonparametric linkage analyses using Affymetrix SNP 6.0 arrays and software for linkage analysis.[16,17] The genomic DNA from Participant II-4 in Family 1 was subjected to four runs in an Illumina Genome Analyzer IIx (100-bp-long paired ends). We used BWA software[18] and SAMtools sequence-alignment mapping[19] with the default settings for alignment and variation detection against the human reference genome (National Center for Biotechnology Information build 36 [also known as hg18]).

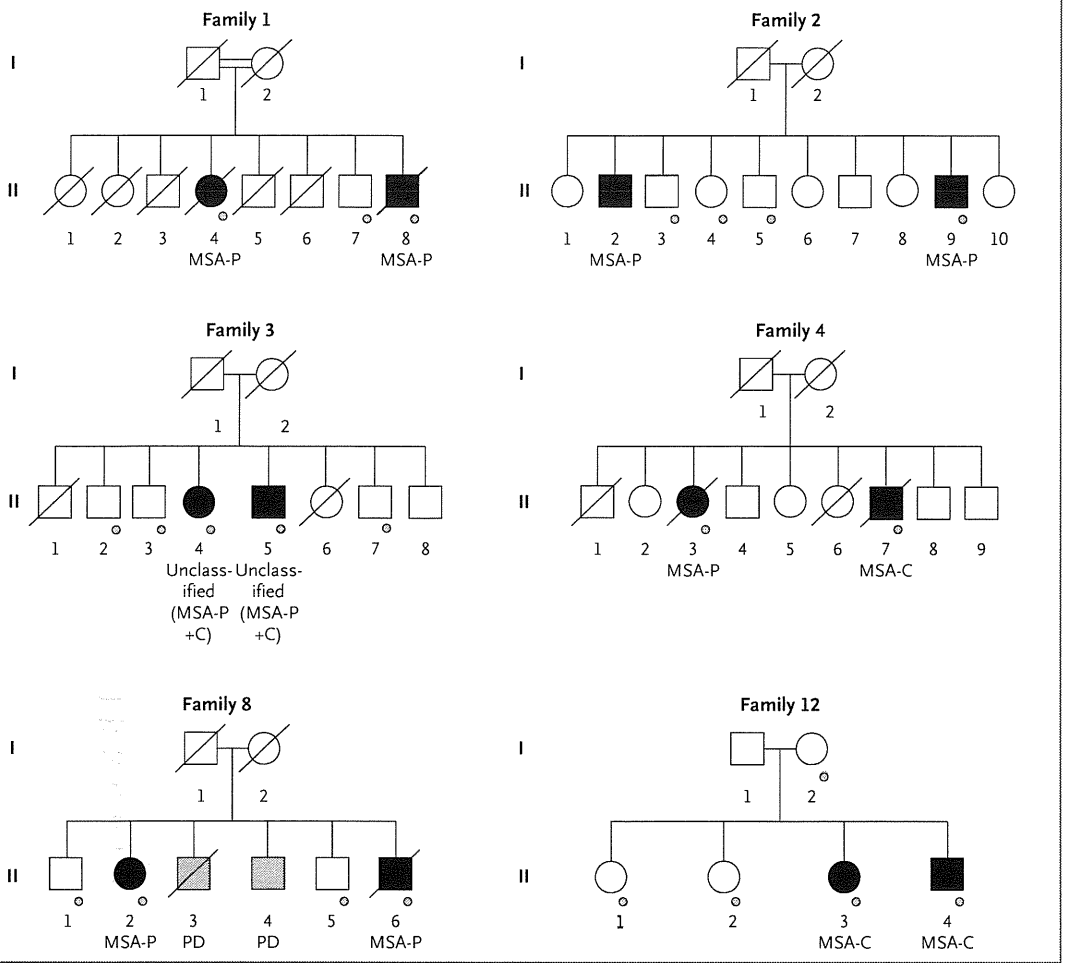

Figure 1. Pedigrees of Six Multiplex Families with Multiple-System Atrophy.

The affected siblings in Family 1 were born to consanguineous parents (first cousins).[13] In this family, the two patients with multiple-system atrophy (Participants II-4 and II-8) also had retinitis pigmentosa, which was not present in the other siblings. The diagnosis of definite multiple-system atrophy in three patients (Participants II-4 and II-8 in Family 1 and II-6 in Family 8) was confirmed at autopsy. In Family 8, two siblings (Participants II-3 and II-4) of the affected family members had Parkinson's disease (PD). In Family 1, in which homozygous M78V-V343A mutations in *COQ2* were identified, the parents (Participants I-1 and I-2), who were obligate carriers of the mutation, showed no overt signs of parkinsonism, cerebellar ataxia, or autonomic dysfunction, according to family report. In Family 12, in whom compound heterozygous R337X/V343A mutations were identified, Participants I-1 and I-2 (obligate carriers of the mutations) and the heterozygous carrier (Participant II-2) showed no overt signs of parkinsonism, cerebellar ataxia, or autonomic dysfunction on examination by a neurologist. Squares represent male family members, circles female family members, black symbols family members with multiple-system atrophy, gray symbols family members with Parkinson's disease, open symbols unaffected family members, slashes deceased family members, and small circles family members for whom genomic DNA samples were available. MSA-C denotes multiple-system atrophy of the cerebellar type, MSA-P multiple-system atrophy with predominant parkinsonism, and unclassified MSA-P+C similarly predominant parkinsonian and cerebellar signs.

ANALYSIS OF *COQ2* AND OTHER GENES ASSOCIATED WITH COENZYME Q_{10}

On the basis of linkage analysis and whole-genome sequencing, we sequenced *COQ2* and the other 11 genes involved in the biosynthetic pathway for coenzyme Q_{10} (*PDSS1*, *PDSS2*, *COQ3*, *COQ4*, *COQ5*, *COQ6*, *COQ7*, *ADCK3*, *COQ9*, *COQ10A*, and *COQ10B*), using the Sanger method (Table S3 in the Supplementary Appendix).

We prepared samples of mutant human *COQ2* complementary DNA (cDNA) by means of site-directed mutagenesis (Table S4 in the Supple-

mentary Appendix). A yeast *coq2*-null mutant, the BY4741Δ*coq2* strain, was transformed with pAUR123 (Takara Bio) containing the nonmutated or mutated human *COQ2* cDNA. We measured the growth rate in a medium with a nonfermentable carbon source by monitoring the optical density of a sample measured at a wavelength of 600 nm (OD_{600}). We used mitochondrial fractions prepared from lymphoblastoid cell lines with the QProteome Mitochondria Isolation Kit (Qiagen) as the enzyme source. COQ2 activity (Enzyme Commission number, 2.5.1.39) was assayed as described previously.[20]

COENZYME Q_{10} LEVEL IN TISSUES

Using high-performance liquid chromatography, we measured levels of coenzyme Q_{10} (ubiquinone-10 and ubiquinol-10) and free (unesterified) cholesterol in lymphoblastoid cell lines established from 152 patients with multiple-system atrophy and 76 controls and in cerebellum samples obtained on autopsy from 3 patients with multiple-system atrophy and 3 controls.[21]

STATISTICAL ANALYSIS

All results are presented as means and standard deviations. We used Student's t-test to evaluate the significance of differences in the mean age at disease onset between carriers and noncarriers of the *COQ2* mutation. We used Fisher's exact test to calculate the significance of the difference in allele frequencies between carriers and noncarriers, with contingency tables and standard methods used to compute odds ratios and corresponding 95% confidence intervals. We used the Kruskal–Wallis test, followed by the Steel test, to perform an analysis of variance. All statistical tests were two-sided, and a P value of less than 0.05 was considered to indicate statistical significance.

RESULTS

LINKAGE ANALYSIS OF FAMILIAL DISEASE

Parametric linkage analysis of the six family pedigrees revealed no single locus showing a linkage compatible with autosomal recessive inheritance. However, in the parametric linkage analysis allowing for heterogeneity, we detected several loci showing positive scores for heterogeneity logarithm of the odds (HLOD), indicating that more than one locus was involved in the different multiplex families (Fig. S1B in the Supplementary Appendix). In particular, two regions on chromosome 4 showed the highest HLOD scores, exceeding 2.0. Results of nonparametric linkage analysis (Fig. S1C in the Supplementary Appendix) were consistent with those of parametric linkage analysis allowing for heterogeneity. Parametric linkage analysis of chromosome 4 in individual pedigrees revealed positive LOD scores in an overlapping region in four families (Family 1, Family 2, Family 4, and Family 12), with Family 1 having the highest LOD score of 1.93 (72.795 to 89.616 Mb) (Fig. S1A and S2A in the Supplementary Appendix). Thus, we selected Family 1 to undergo whole-genome sequencing.

SUSCEPTIBILITY GENE IN FAMILIAL DISEASE

Whole-genome sequencing of a sample obtained from Participant II-4, one of two affected members of Family 1, generated 187.5 Gb of short reads, with an average coverage of 58× and 3,492,429 single-nucleotide variants (SNVs) or insertions or deletions. We winnowed the 3,492,429 variants down to 4 by selecting SNVs that were located in the candidate regions defined on linkage analysis in Family 1 (regions with the highest LOD score spanning approximately 80 Mb in total), that were located in exons or splice sites, that were predicted to cause amino acid changes or changes in pre-messenger RNA splicing, and that were not registered in the database of single-nucleotide polymorphisms, build 130 (dbSNP130), indicating that the variants are extremely rare in the general population (Fig. S2B in the Supplementary Appendix). Each of these 4 SNVs is predicted to result in an amino acid substitution: K707R in SHROOM3 (Universal Protein Resource [UniProt] accession number, Q8TF72), M78V and V343A in COQ2 (UniProt accession number, Q96H96), and R231G in SCEL (UniProt accession number, O95171).

In the 180 Japanese control samples, we did not observe the SNV encoding the M78V variant but did observe SNVs encoding K706R in SHROOM3, V343A in COQ2, and R231G in SCEL, which were present on 3, 5, and 98 of 360 alleles, respectively. We therefore considered the SNP encoding M78V in *COQ2*, which encodes parahydroxybenzoate-polyprenyl transferase, an enzyme involved in the biosynthesis of coenzyme Q_{10}, as a candidate variant in conferring susceptibility to familial multiple-system atrophy.

Cosegregation analysis of samples from Family 1 revealed that the two affected family members, Participants II-4 and II-8, carried the homozygous M78V-V343A variant in *COQ2*, and the unaffected sibling who was tested (Participant II-7) did not carry this variant (Fig. S2C in the Supplementary Appendix). Mutational analysis of *COQ2* in Family 12 revealed heterozygous mutations consisting of nonsense (R337X) and missense (V343A) variants in both affected siblings (Participants II-3 and II-4). Their mother (Participant I-2) was heterozygous for V343A, one unaffected sibling (Participant II-1) lacked this variant, and the other unaffected sibling (Participant II-2) was heterozygous for R337X. R337X was not observed in the 180 Japanese controls.

We did not detect variants of *COQ2* in the other four families (Families 2, 3, 4, and 8). Because *COQ2* encodes an enzyme essential for the biosynthesis of coenzyme Q_{10}, we further sequenced the other 11 genes in the biosynthetic pathway for coenzyme Q_{10} (*PDSS1*, *PDSS2*, *COQ3*, *COQ4*, *COQ5*, *COQ6*, *COQ7*, *ADCK3*, *COQ9*, *COQ10A*, and *COQ10B*) in the remaining four families and in a previously described multiplex family[14] but did not observe variants that cosegregated with disease.

COQ2 VARIANTS AND SPORADIC DISEASE

To investigate the involvement of *COQ2* variants in sporadic multiple-system atrophy, we extended the mutational analysis of *COQ2* to a Japanese series consisting of 363 patients with multiple-system atrophy and 520 controls. A common *COQ2* variant (rs6818847, predicted to result in an amino acid substitution, L16V) with allele frequencies of 0.90 and 0.88 in the Japanese patients with multiple-system atrophy and controls, respectively, was not included in further analysis. Four patients with multiple-system atrophy carried two variants simultaneously (one carried an I97T and a nonmutated [NM] allele at codon 97 and V343A/NM at codon 343, one had R337Q/NM at codon 337 and V343A/NM at codon 343, and two had V343A/V343A), whereas none of the controls had two variants of *COQ2* (Table 1). Sequencing of the subcloned mutated alleles confirmed that R337Q/V343A was present in a compound heterozygous state. We were unable to determine the phase of I97T/V343A, because the distance

Table 1. *COQ2* Variants Found in Patients with Sporadic Multiple-System Atrophy in Japanese, European, and North American Series, as Compared with Controls.*

Genotype	Japanese Series		European Series		North American Series	
	Patients (N=363)	Controls (N=520)	Patients (N=223)	Controls (N=315)	Patients (N=172)	Controls (N=294)
P22L/NM	0	1	0	0	0	0
F29L/NM	0	0	1	0	0	0
P49H†/NM	0	0	0	0	1	0
S57T†/NM	0	0	1	0	0	0
R69H†/NM	0	0	0	0	0	1
I97T‡/V343A§	1	0	0	0	0	0
P107S†/NM	1	0	0	0	0	0
S113F†/NM	1	0	0	0	0	0
T267A‡/NM	0	0	1	0	0	0
S297C‡/NM	0	0	1	0	0	0
N336H/NM	0	1	0	0	0	0
R337Q†/V343A§	1	0	0	0	0	0
V343A§/NM	29	17	0	0	0	0
V343A§/V343A§	2	0	0	0	0	0

* NM denotes nonmutated.
† This variant was deemed to be severely deleterious on yeast complementation assay.
‡ This variant was deemed to be mildly deleterious on yeast complementation assay.
§ This variant had decreased COQ2 activity on enzyme assay.

Table 2. Association between the *COQ2* V343A Variant and Sporadic Multiple-System Atrophy in the Japanese Series.*

V343A Variant†	Patients with Multiple-System Atrophy						Patients with Other Neurologic Diseases		
	Patients (N=363)	Tier 1 Controls (N=520)	Comparison with Tier 1		Tier 2 Controls (N=2383)	Comparison with Tier 2	Alzheimer's Disease (N=2728)	Parkinson's Disease (N=659)	ALS (N=634)
			odds ratio (95% CI)	*P value*		*odds ratio (95% CI)*	*P value*			
Allele frequency — no./total no. (%)	35/726 (4.8)	17/1040 (1.6)	3.05 (1.65–5.85)	1.5×10^{-4}	106/4766 (2.2)	2.23 (1.46–3.32)	6.0×10^{-5}	109/5456 (2.0)	33/1318 (2.5)	31/1268 (2.4)
Heterozygous — no.	31	17			106			105	33	31
Homozygous — no.	2	0			0			2	0	0

* Odds ratios and P values are for the comparisons between patients with multiple-system atrophy and each of the two groups of controls (tier 1 and tier 2). ALS denotes amyotrophic lateral sclerosis, and CI confidence interval.

† In the combined series of Japanese, European, and North American participants, functionally deleterious variants P49H, S57T, R69H, I97T, P107S, S113F, T267A, S297C, and R337Q (as determined on yeast complementation assay) were found in 8 of 1516 alleles (0.53%) in patients with multiple-system atrophy, as compared with 1 of 2258 alleles (0.05%) in controls (odds ratio, 11.97; 95% CI, 1.60 to 531.5; P=0.004).

between I97T and V343A was too large to be amplified by means of polymerase-chain-reaction (PCR) assay in a single fragment, and samples of genomic DNA from the parents were unavailable. We found that 29 patients with multiple-system atrophy and 17 controls were heterozygous for the V343A variant. In addition, we detected four novel heterozygous variants: two in patients with multiple-system atrophy (P107S and S113F) and two in controls (P22L and N336H).

Of the *COQ2* variants, the V343A variant is relatively common in the Japanese population. As shown in Table 2, we found that the V343A allele occurred in 35 of 726 alleles (4.8%) from Japanese patients with multiple-system atrophy and in 17 of 1040 alleles (1.6%) from Japanese controls (odds ratio for patients with multiple-system atrophy, 3.05; 95% confidence interval [CI], 1.65 to 5.85; $P=1.5\times10^{-4}$). Genotyping in the second series of 2383 Japanese controls showed that the V343A variant had an allele frequency of 2.2% (106 of 4766 alleles; odds ratio, 2.23; 95% CI, 1.46 to 3.32; $P=6.0\times10^{-5}$). Genotyping Japanese persons with other neurodegenerative diseases revealed that the V343A allele frequencies were 2.0% (109 of 5456 alleles) among patients with Alzheimer's disease, 2.5% (33 of 1318 alleles) among those with Parkinson's disease, and 2.4% (31 of 1268 alleles) among those with ALS. These allele frequencies did not differ significantly from those in the first or second set of controls, confirming the specificity of the V343A variant in patients with multiple-system atrophy. Two patients with Alzheimer's disease who were found to carry homozygous V343A mutations did not show any signs of parkinsonism, cerebellar ataxia, or autonomic dysfunction.

We then performed genotyping in the European and North American series of patients with multiple-system atrophy. In the European series, we found four singleton *COQ2* variants (encoding amino acid substitutions F29L, S57T, T267A, and S297C) among the patients, whereas none of the controls had any variants in *COQ2*. In the North American series, we found one variant (P49H) in a patient with multiple-system atrophy and one variant (R69H) in a control (Table 1). At the time of recruitment for the study, the carrier of R69H, who was 60 years old, had no signs of parkinsonism, cerebellar ataxia, or autonomic dysfunction, but this participant was unavailable for follow-up assessment. Intriguingly, the V343A

variant, a relatively common variant in the Japanese population, was not observed in patients with multiple-system atrophy or controls in either the European or the North American series.

FUNCTIONAL ANALYSIS OF MUTANT *COQ2*

To determine the functional effect of each variant on the mitochondrial aerobic energy production in which coenzyme Q_{10} plays an essential

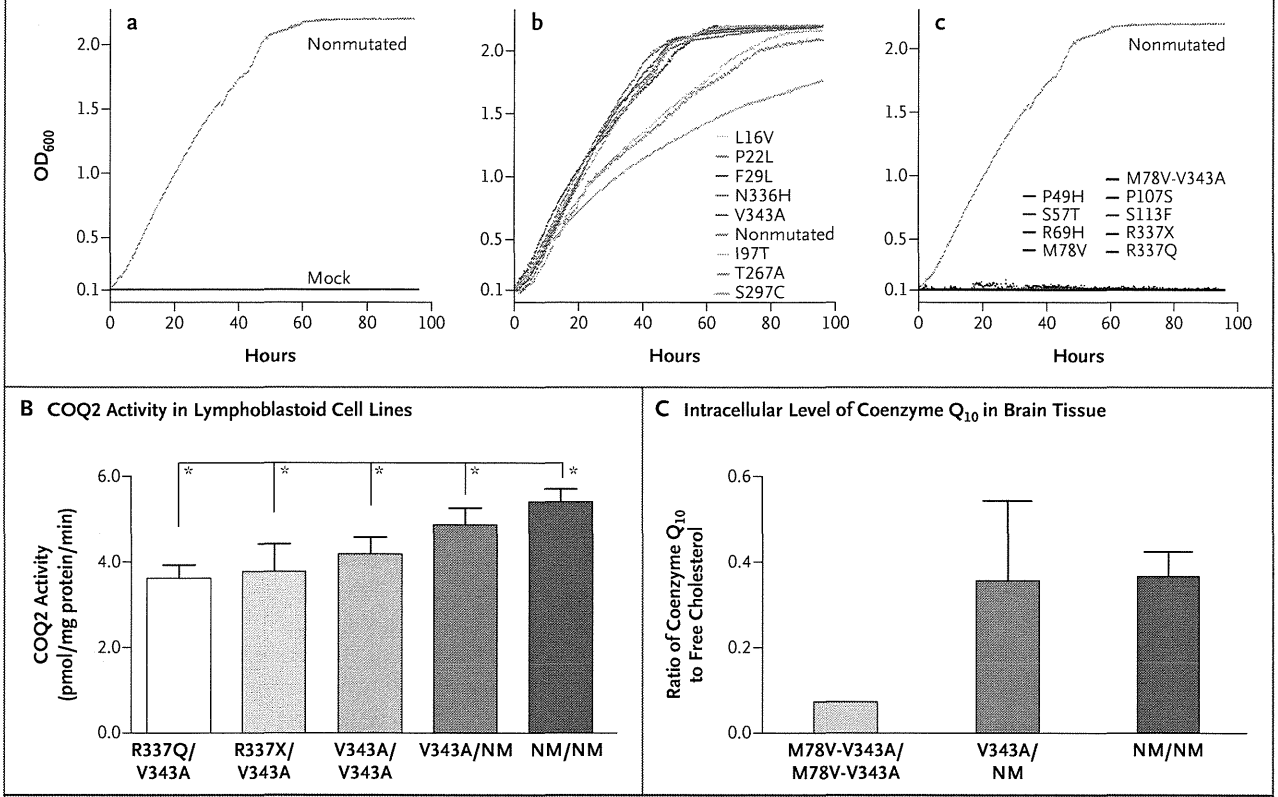

Figure 2. Functional Analysis of *COQ2* Variants.

Panel A shows the results of a yeast complementation assay, including the growth curves of the yeast *coq2*-null mutants transformed with the pAUR123 vector containing the nonmutated (NM) human *COQ2* complementary DNA (cDNA) or mock vector (subpanel a) and those transformed with the AUR123 vector containing different versions of human *COQ2* cDNA (encoding the substitutions L16V, P22L, F29L, N336H, V343A, I97T, T257A, and S297C) (subpanel b). Transformants carrying a *COQ2* allele encoding the I97T, T267A, or S297C substitution show considerably lower growth rates than nonmutated *COQ2*, which still shows a higher growth rate than the *coq2*-null strain (mildly deleterious). Transformants carrying a *COQ2* allele encoding the L16V, P22L, F29L, N336H, or V343A substitution show growth rates similar to that of nonmutated *COQ2*. The *coq2*-null mutants transformed with the pAUR123 vector containing different versions of human *COQ2* cDNA (P49H, S57T, R69H, M78V, M78V-V343A, P107S, S113F, R337X, or R337Q) show severely decreased respiration-dependent growth rates, as does the *coq2*-null strain (severely deleterious) (subpanel c). Each yeast strain was pregrown in yeast extract peptone dextrose (YPD) medium, diluted to an optical density of a sample measured at a wavelength of 600 nm (OD_{600}) of 0.1, and then incubated in yeast extract peptone glycerol (YPG) medium at 23°C with shaking at a rate of 200 rotations per minute for 4 days. OD_{600} was measured every 10 minutes. The experiments were conducted in quadruplicate, and the mean OD_{600} was plotted against the incubation time. Panel B shows COQ2 activity in lymphoblastoid cell lines, as determined by measuring the incorporation of radioactive parahydroxybenzoate (PHB) into decaprenyl-PHB. COQ2 activity was measured in lymphoblastoid cell lines from each patient with multiple-system atrophy carrying *COQ2* variants (encoding R337Q/V343A, R337X/V343A, V343A/V343A, or V343A/NM) and from a control without variants. The mean values from nine independent experiments are shown. T bars indicate standard deviations. Group comparisons were performed with the use of the Kruskal–Wallis test, followed by the Steel test. Asterisks indicate $P<0.05$ for the comparison with a control sample (nonmutated *COQ2* genotype). Panel C shows intracellular levels of coenzyme Q_{10} in frozen cerebellum samples obtained from three patients with multiple-system atrophy (one who was homozygous for M78V-V343A and two who were heterozygous for V343A) and from three controls. Brain-tissue samples weighing approximately 100 mg were homogenized in 10 volumes (volume to weight) of 10 mM TRIS–hydrochloric acid (with a pH of 7.4) containing 0.32 M sucrose, 1 mM ethylenediaminetetraacetic acid (EDTA), and 20% sodium dodecyl sulfate (SDS). Coenzyme Q_{10} was then extracted with hexane and ethanol (in a 5:2 ratio according to volume), and the extract was subjected to high-performance liquid chromatography to measure the level of coenzyme Q_{10}, after adjustment for the free (unesterified) cholesterol level.[21]

role in the electron transfer, we carried out functional complementation analysis by transforming the yeast *coq2*-null strain with nonmutated or mutated human *COQ2* cDNA (Fig. 2A). Transformants of the BY4741 Δ*coq2* yeast strain with the mutated *COQ2*, including transformants separately carrying the P49H, S57T, R69H, M78V, M78V-V343A, P107S, S113F, R337Q, and R337X alleles, showed severely decreased growth rates, similar to those observed in the *coq2*-null strain. In addition, transformants with mutated *COQ2*, including those with the variants encoding the I97T, T267A, and S297C substitutions, showed substantially lower growth rates than those expressing nonmutated *COQ2*, which had a higher growth rate than the *coq2*-null strain (mildly deleterious). The transformants with mutated *COQ2*, including transformants separately carrying the L16V, P22L, F29L, N336H, and V343A alleles, showed growth rates similar to those of the transformants expressing nonmutated *COQ2*. As described above, the yeast strain with M78V-V343A identified in Family 1 showed a severely decreased growth rate, whereas the strain with V343A had a growth rate similar to that of nonmutated *COQ2*, indicating that of the two variants, M78V primarily contributed to the impairment in COQ2 function.

Focusing on the rare variants that were identified in the case–control series (Table 1), we found that nine variants (P49H, S57T, R69H, I97T, P107S, S113F, T267A, S297C, and R337Q) were mildly or severely deleterious. On combining all three series, eight variants (P49H, S57T, I97T, P107S, S113F, T267A, S297C, and R337Q) were identified in 758 patients with multiple-system atrophy, whereas only one variant (R69H) was found in 1129 controls (odds ratio, 11.97; 95% CI, 1.60 to 531.52; P=0.004) (Table 2 footnote). Yeast complementation analysis showed that the F29L variant, identified in a European patient with multiple-system atrophy, did not impair the growth rate. Lymphoblastoid cell lines from this patient were unavailable for further measurement of the activity of mutant COQ2, thus making it difficult to interpret the pathogenicity of this variant.

COQ2 ACTIVITIES IN LYMPHOBLASTOID CELL LINES

We measured COQ2 activities in lymphoblastoid cell lines from patients carrying *COQ2* mutations, when available. We focused on the V343A variant because it is commonly associated with multiple-system atrophy and showed an apparently normal growth rate in the yeast complementation assay. We determined COQ2 activities in lymphoblastoid cell lines with *COQ2* variants R337Q/V343A, R337X/V343A, V343A/V343A, or V343A/NM and in a control without variants. The COQ2 activities in the lymphoblastoid cell lines (V343A/NM) obtained from patients with multiple-system atrophy were significantly lower than those in the control cell lines. The COQ2 activities in the cell lines from patients with multiple-system atrophy carrying two mutated *COQ2* alleles were further decreased (Fig. 2B).

CORRELATIONS BETWEEN GENOTYPE AND PHENOTYPE

The clinical features of patients with sporadic multiple-system atrophy carrying deleterious *COQ2* variants (as determined on yeast complementation assay and COQ2-activity measurement) and those of noncarriers are summarized in Table S5 in the Supplementary Appendix. The mean age at the onset of multiple-system atrophy among carriers was older than that among noncarriers (P=0.002). Among carriers, 34 had subtype C and 5 had subtype P. Among noncarriers, 468 had subtype C and 209 had subtype P. The subtype was unclassified in 42 noncarriers. The ratio of the number of patients with subtype C to the number with subtype P was significantly higher among carriers of *COQ2* variants than among noncarriers (P=0.02).

INTRACELLULAR COENZYME Q_{10} IN LYMPHOBLASTOID CELL LINES

We measured intracellular coenzyme Q_{10} levels in lymphoblastoid cell lines from patients with multiple-system atrophy and controls. The participants were grouped as follows: 3 patients with multiple-system atrophy carrying two variants (R337Q/V343A, R337X/V343A, and V343A/V343A), 16 patients carrying heterozygous V343A, 133 patients without variants, and 76 controls without *COQ2* variants (Table 3). Intracellular levels of coenzyme Q_{10} in lymphoblastoid cell lines from patients with multiple-system atrophy who carried two variant alleles were substantially lower than levels in cell lines from controls without variants. Intracellular coenzyme Q_{10} levels in patients who were heterozygous for V343A and in those without *COQ2* variants were not significantly lower than levels in controls without *COQ2* variants.

Table 3. Intracellular Levels of Coenzyme Q_{10} in Lymphoblastoid Cell Lines, According to *COQ2* Variant.*

Variable	Patients with Multiple-System Atrophy					Controls
	R337Q/V343A	R337X/V343A	V343A/V343A	V343A/NM	NM/NM	NM/NM
No. of participants with variant	1	1	1	16	133	76
Ratio of coenzyme Q_{10} to free (unesterified) cholesterol†	2.19	2.58	1.86	3.38±0.53	3.41±0.74	3.48±0.75
Coenzyme Q_{10} level as a percentage of mean value in controls — %‡	62.9	74.1	53.4	97.1	98.0	100.0

* Plus–minus values are means ±SD. NM denotes nonmutated.

† The ratio of coenzyme Q_{10} to free (unesterified) cholesterol reflects the intracellular level of coenzyme Q_{10}. Lower values indicate decreased levels of intracellular coenzyme Q_{10}, presumably reflecting decreased biosynthesis of coenzyme Q_{10}. To calculate the ratio, coenzyme Q_{10} was measured in nanomoles per liter and free cholesterol in micromoles per liter.

‡ Lower values indicate decreased levels of intracellular coenzyme Q_{10}, as compared with the mean value in controls, presumably reflecting decreased biosynthesis of coenzyme Q_{10}.

COENZYME Q_{10} IN BRAIN TISSUE

Only a limited number of brain-tissue samples from patients with multiple-system atrophy carrying *COQ2* variants were available. Nevertheless, we measured coenzyme Q_{10} in frozen brain tissues from three patients with *COQ2* variants (one patient who was homozygous for M78V-V343A and two patients with V343A/NM) and from three controls without *COQ2* variants (Fig. 2C). The levels of coenzyme Q_{10} in patients who were homozygous for M78V-V343A were substantially lower than the levels in controls.

DISCUSSION

We identified homozygous or compound heterozygous *COQ2* mutations in two of the six multiplex families with multiple-system atrophy, a finding that suggests a role of these mutations in the pathogenesis of familial disease. We further found that functionally impaired variants in *COQ2* were associated with an increased risk of sporadic disease. In familial cases of multiple-system atrophy, linkage analysis strongly indicated locus heterogeneity in these families, and the identification of the causal variants in the remaining four families will require analyses such as whole-genome sequencing.

We found that a common variant (V343A) and multiple rare variants in *COQ2* were associated with sporadic multiple-system atrophy. The V343A variant was found exclusively in the Japanese participants, with an allele frequency of 1.6 to 2.2%. The allele frequency of V343A in patients with multiple-system atrophy (4.8%) was significantly higher than that in controls (1.6 to 2.2%) with odds ratios of 2.23 to 3.05. The modest risk of multiple-system atrophy that was associated with the common variant V343A suggests that V343A is a susceptibility factor rather than a causal factor for this disease. The odds ratio for the presence of deleterious rare variants was 11.97, which is much larger than that for V343A. Nonetheless, we should consider that these heterozygous variants in *COQ2* are not necessarily causal but rather confer a strong susceptibility to sporadic multiple-system atrophy. Members of Family 1 and Family 12 who carried deleterious variants in the heterozygous state did not have clinical signs of multiple-system atrophy.

The ratio of patients with subtype C multiple-system atrophy to those with subtype P was higher among carriers of deleterious *COQ2* variants than among noncarriers, which suggests that the cerebellum is more vulnerable to compromised COQ2 function than other regions of the central nervous system. Of the *COQ2* variants that we detected, the V343A variant was the most prevalent and was exclusively found in Japanese participants. These findings may in part explain the clinical observations that subtype C is more prevalent than subtype P in the Japanese population[9] but not in the European population[11] or the North American population.[12] However, there were only 35 carriers of deleterious *COQ2* variants among 363 patients with multiple-system atrophy in the Japanese case series. In addition, the clinical presentations of the two patients with familial